Icarus 226 (2013) 256–267

Contents lists available at SciVerse ScienceDirect

Icarus

journal homepage: www.elsevier.com/locate/icarus

The D/H ratio of water in the solar nebula during its formation and evolution

Le Yang [a,*], Fred J. Ciesla [a], Conel M.O'D. Alexander [b]

[a] Department of the Geophysical Sciences, The University of Chicago, 5734 South Ellis Avenue, Chicago, IL 60637, USA
[b] DTM, Carnegie Institution of Washington, Washington, DC 20015, USA

ARTICLE INFO

Article history:
Received 25 January 2013
Revised 6 May 2013
Accepted 15 May 2013
Available online 7 June 2013

Keywords:
Cosmochemistry
Comets, Composition
Origin, Solar System
Solar nebula

ABSTRACT

We couple a dynamic model of material transport and mixing within a forming and evolving protoplanetary disk with a kinetic study of D–H isotopic exchange amongst gas-phase molecules to explore the isotopic evolution of water in a young protoplanetary system. We begin with water that was highly deuterated in the parent molecular cloud core, then track its isotopic evolution within the protoplanetary disk. Our model shows the $(D/H)_{water}$ is low in the hot inner disk due to rapid isotopic exchange with molecular hydrogen, and then increases toward the cold, outer disk where exchange reactions are more sluggish. These results are consistent with previous studies. However, counter to previous studies, we find that the $(D/H)_{water}$ decreases again in the outer regions of the disk because water that exchanged at high temperatures near the young star would have been transported outward during the early evolution of the disk. As a result, water ice in the outermost region of the disk may have, on average, a lower $(D/H)_{water}$ ratio than found closer to the star. This non-monotonic gradient in D/H could explain the recent observations showing that the $(D/H)_{water}$ of a Jupiter Family Comet, 103P/Hartley 2, is lower than that of previously measured Oort cloud comets.

1. Introduction

In the last decade, theoretical studies of interstellar chemistry have revealed that water becomes enriched in deuterium relative to molecular hydrogen through ion–molecule and grain surface reactions at $T < 50$ K in astrophysical environments (Brown and Millar, 1989; Millar et al., 1989; Roberts and Millar, 2000; Roberts et al., 2004). These models predict that water in molecular cloud cores, where temperatures may be 10–20 K, develops D/H ratios ranging from 0.001 to 0.01, which are about 2–3 orders of magnitude higher than the cosmic (D/H) value ($\sim 1.6 \times 10^{-5}$; Linsky, 2003) and also greater than the bulk solar (D/H) value ($\sim 2 \times 10^{-5}$; Geiss and Gloeckler, 1998). This prediction is supported by astronomical observations showing that the $(D/H)_{water}$ in hot cores ($T \sim 100$–200 K) where water ice is being evaporated are $\sim 3 \times 10^{-4}$–3×10^{-2} (Jacq et al., 1990; Gensheimer et al., 1996; Rodgers and Millar, 1996; Lerate et al., 2006; Persson et al., 2007; Bergin et al., 2010; Liu et al., 2011; Coutens et al., 2012).

However, such high D/H values are not necessarily preserved in water throughout the process of planet formation. When water is incorporated into the hot, inner region of a protoplanetary disk, it would undergo isotopic exchange reactions with other hydrogen-bearing species, erasing some, or all, of the memory of the molecular cloud. This process was examined in a number of studies that modeled how deuterated water was processed and redistributed in viscously evolving disks (e.g., Drouart et al., 1999; Mousis et al., 2000; Hersant et al., 2001; Horner et al., 2007; Kavelaars et al., 2011; Petit et al., 2011). These studies allowed for isotopic exchange via the reaction $H_2O + HD \leftrightarrow HDO + H_2$ (Geiss and Reeves, 1981; Lécluse and Robert, 1994) in the various environments found in the solar nebula in order to determine how the isotopic composition of water would vary across the Solar System. Because isotopic exchange occurred rapidly at high temperatures, these models found that water would equilibrate with the hydrogen and acquire a $(D/H)_{water} \sim 2 \times 10^{-5}$ in the inner regions of the nebula. While in the outer disk, where low temperatures led to sluggish isotopic exchange, water would preserve its high $(D/H)_{water}$ ratio. While the details of these models varied depending on the assumed initial conditions, their overall results generally agreed with available data of the D/H ratio of water-bearing Solar System bodies. In particular, it was found that water in Oort cloud comets, which may have formed amongst the giant planets, had greater deuterium enrichments than found in Earth's water or the aqueously altered meteorites, all of which were thought to form closer to the Sun (Balsiger et al., 1995; Bockelée-Morvan et al., 1998; De Laeter et al., 2003; Robert, 2006).

* Corresponding author.
E-mail address: leyang@uchicago.edu (L. Yang).

0019-1035/$ - see front matter © 2013 Elsevier Inc. All rights reserved.
http://dx.doi.org/10.1016/j.icarus.2013.05.027

These models have recently been challenged by the Herschel/HIFI observations of a Jupiter Family Comet (JFC), 103P/Hartley 2 (Hartogh et al., 2011). Being a JFC, Hartley 2 may have originated beyond the region where Neptune formed (Dones et al., 2004; Morbidelli, 2005; Duncan, 2008). While it is uncertain exactly where Oort cloud comets formed (e.g., Dones et al., 2004; Levison et al., 2010; Brasser et al., 2012) the similar D/H ratio of these comets and water from Saturn's moon Enceladus (Waite et al., 2009) supports the theory that they formed in the Jupiter and Saturn forming regions. As the JFCs may have formed beyond this region, the models described above would predict that the $(D/H)_{water}$ in the JFCs would be equal to or greater than what is seen in the Oort cloud comets. However, the D/H value of water in Hartley 2 was found to be $1.61 \pm 0.24 \times 10^{-4}$, approximately a factor of two lower than those values measured in Oort cloud comets ($\sim 3 \times 10^{-4}$; Balsiger et al., 1995; Bockelée-Morvan et al., 1998, 2012; Meier et al., 1998; Villanueva et al., 2009; Brown et al., 2012) and comparable to what is found in the Earth's oceans today.

If Hartley 2 is representative of other JFCs, we must ask whether it is possible for the D/H variations in water ice in the outer nebula to be less than those found in the giant planet formation region. Here we attempt to address this by extending previous models to consider the time period prior to when other models began. That is, previous modeling efforts began their simulations with a fully formed solar nebula that was no longer accreting mass from its parent molecular cloud. However, solar nebula formation is expected to occur over a finite period of time, resulting in materials being processed and redistributed prior to the time the disk reached its final mass. As a result, materials processed at high temperatures can be pushed outwards by disk early evolution, before being diluted by freshly added cloud materials (Dullemond et al., 2006; Yang and Ciesla, 2012). Here, we revisit the dynamical and isotopic evolution of water in the early solar nebula and explicitly consider the effects of disk building in order to evaluate how this would impact the isotopic distribution of water in the solar nebula.

In the next section, we present the model used here, describing both the physical and chemical models that we used in our study. We then apply the model to explore how $(D/H)_{water}$ varies within an early evolving disk. Following that, we discuss how variations in key parameters would affect the results. We end with a discussion of how our results could be applied to interpret previous measurements, and how our model could be tested by future studies of meteoritic and cometary materials.

2. Model description

We consider a disk forming within its parent molecular cloud core as it undergoes inside-out collapse (Shu, 1977), and its evolution as mass and angular momentum are redistributed by internal processes. Assuming that materials within the molecular cloud are well mixed prior to infall, water, whose D/H ratio would be enhanced over the bulk value for the cloud (Roberts and Millar, 2000; Roberts et al., 2004), would be accreted into the star + disk system as a constant fraction of the infalling materials. Where infalling materials are added to the disk depends on the specific angular momentum that each parcel of material had in the parent cloud (Hueso and Guillot, 2005). Once incorporated into the disk, the water would be redistributed in the solar nebula through viscous evolution, along with other hydrogen-bearing species and their deuterium isotopologues, most notably H_2, HD, OH, and OD. Since those gaseous materials see different environments (temperature and pressure) throughout the course of disk evolution, water would undergo isotopic exchange with these other species at rates that depend on their locations in the disk.

2.1. Disk model

Our dynamic model calculates how the surface density profile, $\Sigma(R, t)$, changes with time as the disk evolves as a result of angular momentum transport during and after the period when the disk accreted material from its parent molecular cloud. Here we qualitatively describe the physical effects that determine how the disk evolves. Detailed equations and treatments can be found in Yang and Ciesla (2012), which adopted many of the same methodologies used in previous models (e.g., Hueso and Guillot, 2005; Dullemond et al., 2006; Zhu et al., 2010).

During the period of disk building, infalling materials from the molecular cloud are added to and well mixed-vertically within the disk at locations inside the centrifugal radius, which is defined as the distance from the central protostar where the orbital angular momentum of the material in the disk equals the maximum angular momentum in the shell of molecular cloud core being accreted at that time (Dullemond et al., 2006; Hueso and Guillot, 2005; Zhu et al., 2010). Some of the mass inside of the centrifugal radius is pushed outwards due to the viscous spreading associated with angular momentum conservation. Viscous evolution continues even after infall ceases.

Here, we adopt the classical α-viscosity formalism (Shakura and Sunyaev, 1973; Lynden-Bell and Pringle, 1974), as this provides a computationally simple method for representing the mass and angular momentum evolution of the disk over long timescales. Here we assume that the turbulent viscous parameter, α, has a uniform value of 0.001, but can be augmented in gravitationally unstable regions (Armitage et al., 2001). We will return to discuss how different values of α would affect our results later.

All gaseous species involved in the D–H exchange reaction network are transported by advection and diffusion within the disk:

$$\frac{\partial \Sigma_i}{\partial t} + \frac{1}{R}\frac{\partial R \Sigma_i v_r}{\partial R} = \frac{1}{R}\frac{\partial}{\partial R}\left[RD\Sigma \frac{\partial}{\partial R}\left(\frac{\Sigma_i}{\Sigma}\right)\right] + S_i(R,t) \quad (1)$$

where Σ_i is the surface density of gaseous species that are considered. D is the diffusion coefficient, which is assumed to be equal to the viscosity ν. $S_i(R, t)$ is the source term of a specific gaseous species that is added from infall, if applicable, and also that is altered through the chemical reaction network that is described in the following section.

The thermal evolution of the disk is determined by balancing the energy received from viscous dissipation, irradiation from the central star, and radiation from the cloud envelope with the energy lost from the disk surface. In our calculations, disk opacity is dominated by dust, and thus is assigned a low value in regions above the dust sublimation temperature (for details see Yang and Ciesla, 2012).

2.2. Chemical model

In the models of Drouart et al. (1999) and Mousis et al. (2000), isotope exchange between water and hydrogen was assumed to be determined by the reaction $H_2O + HD \leftrightarrow HDO + H_2$, with the forward and backward reaction rates provided by Lécluse and Robert (1994). More recent studies (e.g., Willacy, 2007; Willacy and Woods, 2009; Thi et al., 2010) have explored how this D–H exchange would have occurred by considering a suite of possible reactions involving the major chemical species that would have been present in the solar nebula gas. This was done because water molecules would not have been limited to react with just H_2 in the disk, and the water abundance would vary with temperature.

As shown by Thi et al. (2010), water deuteration would have strongly depended on the behavior of the hydroxyl radical, OH.

The hydroxyl radical can be deuterated through the exchange reaction:

$$D + OH \leftrightarrow OD + H \quad (2)$$

while the reverse reaction has a much higher activation barrier than the forward reaction (Yung et al., 1988). Water that formed through reactions involving the hydroxyl radical, such as $OD + H_2 \rightarrow HDO + H$ and $OD + OH \rightarrow HDO + O$, would thus inherit the deuteration. The work of Thi et al. (2010) and others did not include the $H_2O + HD \leftrightarrow HDO + H_2$ reaction, but D–H exchange involving water and molecular hydrogen can proceed through a variety of intermediate reactions involving other radicals. Since our model focuses on the early stage of disk evolution when the effects of photochemistry and ion-molecular reactions are diluted significantly in the massive disk, we, for now, consider only neutral–neutral reactions (a list of all reactions included in our network is provided in Appendix A).

Our model considers the 13 gaseous species: H_2, HD, H, D, OH, OD, H_2O, HDO, O, O_2, CO, CO_2, and C that are involved in reactions that control isotopic exchange between water and molecular hydrogen and their abundances (He is also included to serve as a third body in some reactions). The rate of change in the abundance for each species in our model is given by:

$$\frac{d[i]}{dt} = \sum_{j,k} \beta_{jk}[j][k] - \sum_{k} \beta_{ik}[i][k] \quad (3)$$

where $[i]$, $[j]$ and $[k]$ are the number densities of species i, j, and k while β_{jk} and β_{ik} are the rate coefficients of reactions for which species i is a product or a reactant, respectively. The reaction rate coefficients are taken from the UMIST database (Woodall et al., 2007) when available. Reaction rate coefficients involving deuterated species are either from chemical kinetic studies (Yung et al., 1988; Zhang and Miller, 1989; Talukdar et al., 1996) or assumed to be equal to the rates involving H isotopologues when no literature values are available, as done in Willacy (2007) and Thi et al. (2010). A detailed comparison of our network with the reaction used in Drouart et al. (1999) and Mousis et al. (2000) is presented in Appendix A. While differences exist between the predicted rates of exchange, the main conclusions of our study remain true regardless of whether we use our chemical network or the single exchange reaction of Lécluse and Robert (1994).

2.3. Deuterium chemistry evaluated under solar nebula conditions

The changes in abundances of the various species considered here are determined by Eq. (1) using the conditions present at the disk midplane. The number density of each species in Eq. (3) is related to its surface density by

$$[i] = \frac{\Sigma_i}{\sqrt{2\pi}H} \Big/ m_i \quad (4)$$

where m_i is the molecular mass of species i, and H is the disk vertical scale height, with $H = C_s/\Omega_k$ (where Ω_k is the local Keplerian frequency and C_s is the local speed of sound).

When water exchanges deuterium with molecular hydrogen via our chemical reaction network, the reaction rates are strong functions of pressure, temperature, and the abundances of the reactants, each of which changes with location and time as the disk evolves. The higher the temperature (and also the density) is, the faster the exchange proceeds. Fig. 1 illustrates these effects as it shows how the $(D/H)_{water}$ would change with time under a variety of disk conditions. In regions where the gas pressure ranges from 10^{-3} to 10^{-5} bar, which is typical of the high temperature inner regions of the solar nebula, the $(D/H)_{water}$ decreases quickly, reaching the equilibrated value within ~1 year. At lower temperatures (800 K > T > 300 K), the timescale for water to reach a steady-state value increases. For example, the upper-right panel of Fig. 1 shows the evolution of $(D/H)_{water}$ at T = 600 K. When T is below 300 K, isotope exchange is too slow to reach the equilibrium value within the evolutionary timescale of a protoplanetary disk regardless of the pressure. This means that D–H exchange would proceed efficiently in the hot inner region of disk, and be minimal at greater distances from the young Sun, where water ice is likely to form. It is worthwhile to note that the system reaches equilibrium faster through our chemistry network than if we only consider the net reaction $H_2O + HD \leftrightarrow HDO + H_2$ and the rate coefficients of Lécluse and Robert (1994). Again, this is discussed in Appendix A.

Our initial configuration involves material falling inward from a parent molecular cloud. The assumed composition of this material generally follows Willacy and Woods (2009), where the initial abundances of species were determined by modeling the chemical evolution under molecular cloud conditions for 1 Myr. We have modified the initial abundances of the species as we have adopted different estimates for the elemental abundances recommended by Lodders (2010) for the Solar System (Tables 1 and 2). Given that the $(D/H)_{water}$ in molecular clouds is estimated to be 3×10^{-4}–3×10^{-2} from both observations and theoretical calculations (Gensheimer et al., 1996; Robert, 2006; Millar, 2002; Liu et al., 2011; Coutens et al., 2012), we choose 0.001 as a typical value for $(D/H)_{water}$ in the cloud core. While the exact numerical values of $(D/H)_{water}$ may thus differ from what is reported here, the trends that we find are robust. We discuss this issue further below.

2.4. Numerical approach

A step-wise summary of our model is provided in Fig. 2. In our model, those equations describing the $\Sigma(R, t)$ evolution are solved using an explicit finite-difference scheme, as described in Yang and Ciesla (2012). The computational grid for the disk is made of 60 annuli with the first annulus centered on 0.05 AU. The radial distance between the n + 1st and nth annulus is $1.1^n \times 0.1$ AU until the nth annulus is nearly 50 AU away from the central star. Beyond that, the radial distance between adjacent annuli is $1.1^n \times 0.5$ AU. The farthest annulus is ~1000 AU away. Equations describing the disk properties are then solved during each timestep to give the local physical conditions (midplane temperature and density).

The chemical evolution of the system is evaluated at the disk midplane at locations where the temperature exceeds 160 K. We do this because at lower temperatures water condenses as water ice. Although the exact condensation temperature varies with pressure, the chemical reactions are so sluggish at these low temperatures that the exact choice here has little impact on the results. We solve Eq. (3) for each species implicitly by using a backward Euler method during every timestep. The new surface density of each species at location R is taken as the initial value of the next timestep. Calculations are then repeated to compute the first 1 Myr of disk evolution.

3. Model results

3.1. Solar nebula evolution

In our model, solar nebula formation and evolution is primarily characterized by three parameters: the initial angular velocity of parent cloud, ω_{cd}, which controls the fraction of the cloud mass that is incorporated into the protoplanetary disk, the molecular cloud temperature, T_{cd}, which determines the mass accretion rate from the cloud core to the star-disk system, and the viscous parameter, α, which characterizes the viscous evolution (for details see: Hueso and Guillot, 2005; Dullemond et al., 2006; Yang and Ciesla, 2012). The values used in our standard case are shown in Table 3,

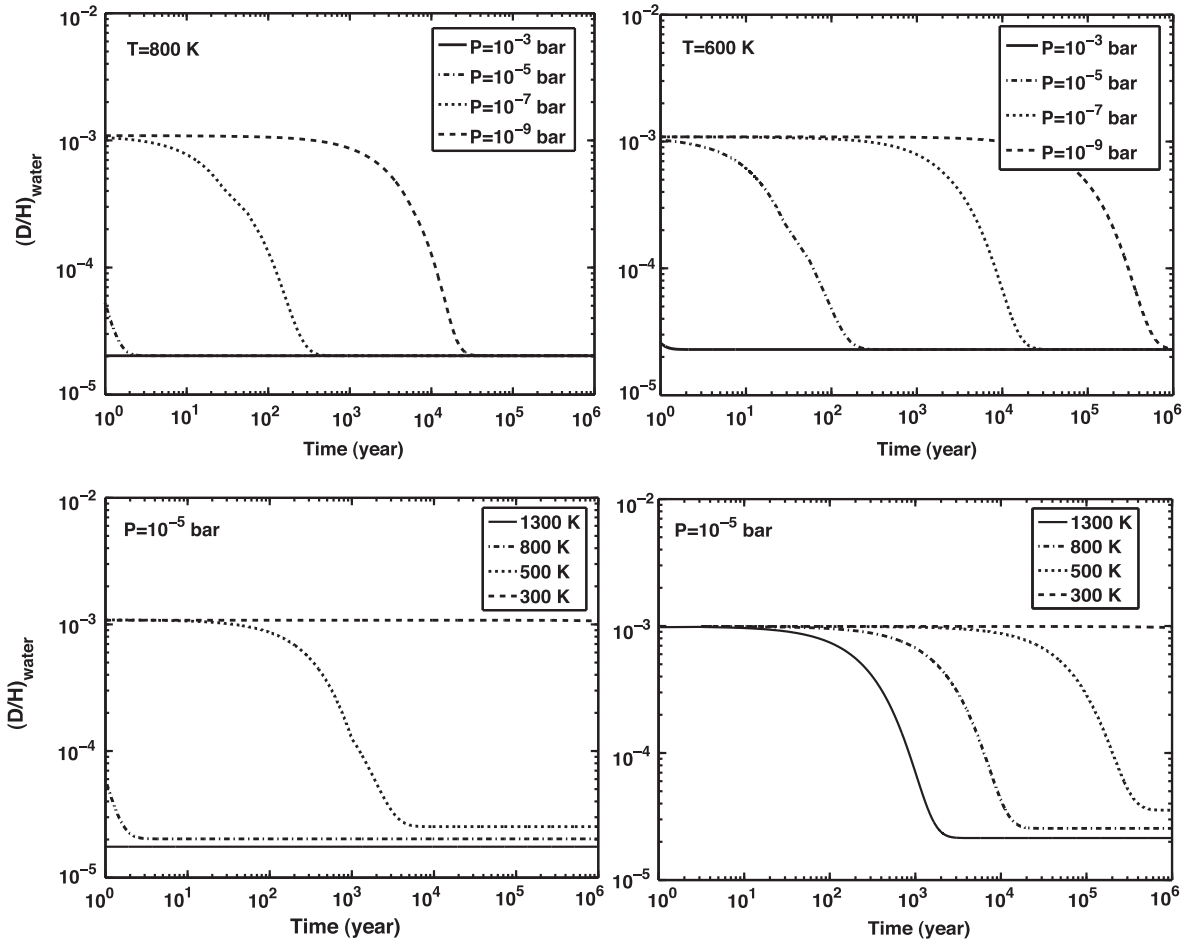

Fig. 1. The evolution of the water (D/H) ratio at various temperatures and pressures. The top panels show how the isotopic evolution proceeds at different pressures, but constant temperatures using our chemical network. The lower left panel shows the effect of temperature on the reaction rate. For comparison, the lower-right panel shows how the $(D/H)_{water}$ would evolve with time if only considering the reaction $H_2O + HD \leftrightarrow HDO + H_2$ and the rates from Lécluse and Robert (1994).

Table 1
Elemental abundances with respect to the total number density of hydrogen nuclei n_H which is equal to $[H] + 2[H_2]$.

Element	Abundance
H	1
D	1.94×10^{-5} [1, 2]
O	4.68×10^{-4} [2]
C	2.48×10^{-4} [2]
He	0.097 [2]

[1] Geiss and Gloeckler (1998); [2] Lodders (2010).

Table 2
Initial fractional abundances with respect to the total number of hydrogen nuclei n_H.

Chemical species	Abundance
H	2.8×10^{-5} [1]
H_2	0.49999 [1]
D	6.7×10^{-7} [2]
HD	1.9×10^{-5} [3]
He	0.097 [4]
H_2O	2.2×10^{-4} [2]
HDO	4.4×10^{-7} [5]
OH	2.4×10^{-8} [1]
OD	4.1×10^{-8} [1]
O	8.5×10^{-7} [1]
O_2	4.4×10^{-8} [1]
C	3.9×10^{-7} [1]
CO	2.5×10^{-4} [2]
CO_2	2.8×10^{-7} [1]

[1] Willacy and Woods (2009); [2] Calculated based on mass balance; [3] Geiss and Gloeckler (1998); [4] Lodders (2010); [5] Calculated based on the assumed initial $(D/H)_{water}$ in the molecular cloud.

and the typical ranges for those parameters are also provided for reference. How variations in those parameters affect the solar nebula evolution and also the $(D/H)_{water}$ distribution in the solar nebula will be discussed below.

Here, disk evolution is represented by how its mass, the surface density profile and the midplane temperature profile evolve with time. During the infall stage when molecular cloud materials are added to the star + disk system, the disk mass increases with time and reaches its maximum value at the time that infall stops (t = 0.3 Myr in our standard case), as shown in the upper-left panel of Fig. 3. As the molecular cloud undergoes inside-out collapse, the centrifugal radius increases with time and reaches about 10 AU when infall stops. Since infalling materials are added at locations inside the centrifugal radius, all mass located outside of the centrifugal radius arrived there through outward transport by viscous spreading within the disk. In the meantime, some of the disk materials from the inner region are pushed inwards due to viscous stresses, and accreted by the young Sun. This process will proceed continuously even after infall stops, resulting in the disk decreasing in mass, and expanding radially with time, as shown in Fig. 3.

The evolution of the disk midplane temperature generally follows that of the disk surface density: temperatures rise with increasing surface density, and decrease when the surface density drops. This is because higher surface densities lead to higher rates

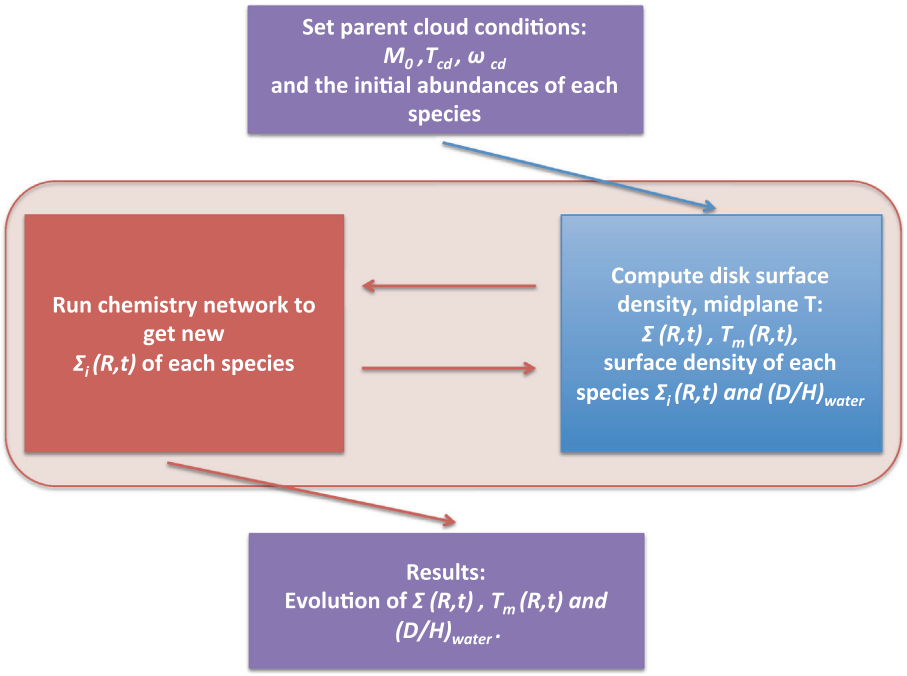

Fig. 2. Step-wise summary of our model.

Table 3
The main disk model parameters.

Parameter	Values used in the standard model	Typical values
ω_{cd}	10^{-14} s^{-1}	10^{-15}–10^{-13} s^{-1} [1]
T_{cd}	15 K	10–20 K [2]
α	0.001	10^{-5}–0.1 [3]

[1] Goodman et al. (1993) and Lodato (2008); [2] van Dishoeck et al. (1993); [3] Hartmann et al. (1998) and Hueso and Guillot (2005).

of heat production and more effective trapping of dissipated energy. As a result, the snowline, which is found where $T \sim 160$ K, moves further away from the central star during infall, and moves inward once infall ceases, as the disk decreases in mass and cools. After 2 Myr of disk evolution in our model, the snowline is located at ~5 AU. As shown, an isothermal region with a temperature of ~1300 K develops in the disk and extends from ~0.3 AU to 2 AU at various times in the lifetime of the disk. This isothermal behavior is because most of the silicate dust evaporates around the midplane in these regions, which dramatically reduces the opacity, and leads to very small temperature gradients (see also Cassen, 1994, 2001).

3.2. The distribution of $(D/H)_{water}$ in a protoplanetary disk

We calculated how the $(D/H)_{water}$ varies with location in the disk within the first 1 Myr of disk formation and evolution. Results are shown in Fig. 4. During the early stage of infall, the deuterated water from the molecular cloud falls into the innermost region, and rapidly equilibrates with molecular hydrogen due to rapid isotopic exchange expected at high temperatures there. As shown, the $(D/H)_{water}$ inside of 2 AU almost equals that of molecular hydrogen. Some of that equilibrated water gets pushed outwards and redistributed throughout the rest of the disk by viscous spreading. At later times during the infall stage, deuterated water from the molecular cloud continues to be incorporated into the hot inner region, in addition to the cooler, outer region. In this outer region, the deuterated water mixes with deuterium-poor water that had been transported there from the hot inner disk. As shown in Fig. 4, the net $(D/H)_{water}$ in the disk reaches maximum values at ~3 AU and ~10 AU in the 0.2 Myr and 0.3 Myr snapshots, respectively, due to the freshly added water from the molecular cloud. At the same time, the $(D/H)_{water}$ decreases further away from the Sun, reaching values as low as that of molecular hydrogen again–the same values as achieved very close to the Sun. This is the water that was first incorporated into the disk, underwent D–H exchange close to the Sun, and was then transported outward during early viscous evolution. Due to the low temperatures and minimal isotopic exchange expected in the outer regions, the low $(D/H)_{water}$ of this originally inner disk water is preserved there. As a result, the $(D/H)_{water}$ does not monotonically increase away from the central star at these early epochs, unlike the predictions of previous studies (e.g., Drouart et al., 1999; Mousis et al., 2000).

Once infall stopped, water, as well as other gaseous species, continues to diffuse and be advected throughout the disk while undergoing isotopic exchange with other gaseous species. The net result is that the peak in the radial distribution of $(D/H)_{water}$ decreases with time, and the net $(D/H)_{water}$ in the outer region of the disk becomes more uniform due to the mixing processes. However, even with this mixing, the non-monotonic distribution of $(D/H)_{water}$ can still persist for over 1 Myr of disk evolution.

As disk evolution slows after infall ceases, the turbulence in the disk may decrease in certain regions due to low ionization levels, preventing the development of the MRI (e.g., Gammie, 1996) or the disk evolving away from a gravitationally unstable state. As a result, dust growth will become more efficient, allowing grains containing water ice to aggregate and drift inwards due to gas drag (Weidenschilling, 1977). As these bodies cross the snow line, water ice will evaporate (Cyr et al., 1998; Cuzzi and Zahnle, 2004; Ciesla and Cuzzi, 2006). The resulting water vapor will then undergo isotopic exchange if it flows inwards into regions that are warm enough, as well as diffuse outwards again to freeze out as water ice. This would likely alter the D/H distribution of water around the snowline (e.g., Jacquet and Robert, 2013), though the details will depend critically on how dust growth proceeds in the outer disk. Since we focus on the first ~1 Myr of infall and disk evolution before such effects are expected to have become important, we do not account for this in our model.

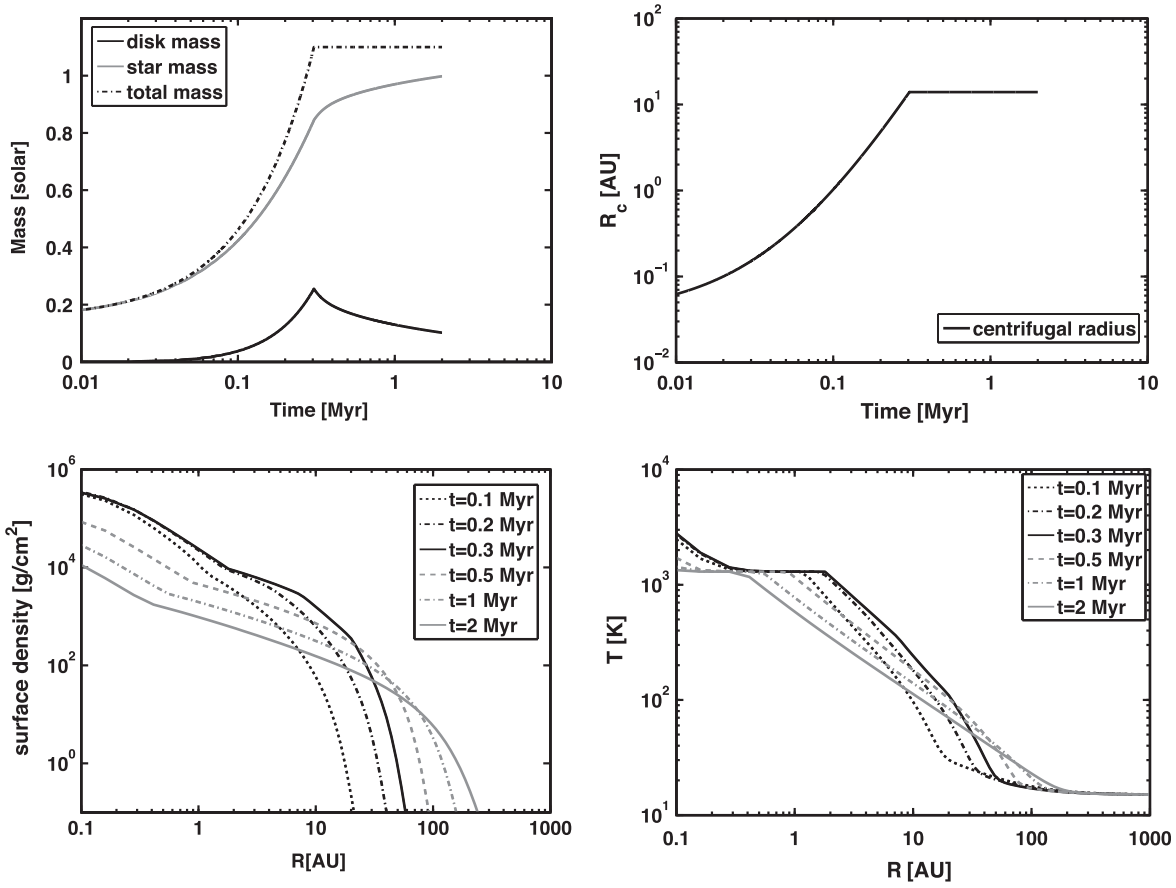

Fig. 3. The upper two figures show how the disk mass, star mass, total mass (the left plot) and the centrifugal radius (the right plot) evolve with time. The total mass of the parent cloud is 1.1 Solar Mass, which is chosen in order to make the mass of the central star close to 1 Solar Mass at end of the simulation. The lower two figures show the disk surface density (left) and the disk midplane temperature (right) versus distance from the Sun at different times. Infall stops at 0.3 Myr.

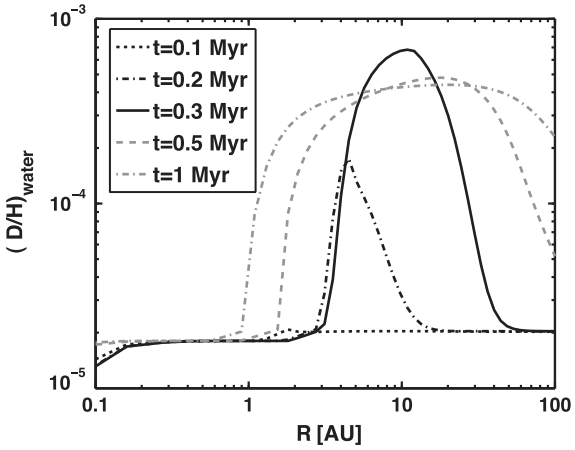

Fig. 4. The radial distribution of $(D/H)_{water}$ in the solar nebula at different times in the standard model presented here. Black lines represent times when infall continues, while gray lines are for times after infall has ceased (at ~0.3 Myr).

3.3. Possible variations in model results caused by different parameter values

Since our model combines a kinetic study of the D–H exchange reaction network with the dynamical model of disk formation and evolution, model results will vary depending on the choice of initial parameters related to either the deuterium chemistry, or the molecular cloud and disk models. The effects of variations in these parameters on the evolution and transport of materials were considered in detail by Yang and Ciesla (2012). Here we summarize the effects that changes in these parameters or initial conditions have on the results of this study.

ω_{cd} determines the fraction of deuterated water that falls into the hot, inner region to undergo isotopic exchange, and the fraction that falls onto the outer disk preserving its elevated D/H ratio. In the case with higher ω_{cd}, less water is processed at high temperatures in the disk, since materials would fall further from the star due to the greater angular momentum, whereas lower values lead to greater amounts of processing. Regardless, viscous spreading would allow early processed materials to be pushed outwards during infall and the non-monotonic distribution of $(D/H)_{water}$ will still develop, with the spatial gradients being determined by this choice of parameter.

T_{cd} mainly affects the infall rate of mass from the molecular cloud core onto the star-disk system. Hotter clouds collapse on shorter timescales, and thus, the predicted non-monotonic distribution of $(D/H)_{water}$ will develop a few hundreds of thousands years earlier compared to our standard case. However, different values of T_{cd} will not change the distribution of the materials falling into the disk provided that the centrifugal radius stays the same. Consequently, the shape and values of the $(D/H)_{water}$ distribution in the solar nebula will hardly be affected by varying the T_{cd}.

The last parameter α, which determines the magnitude of viscosity in our model, influences how materials are transported in the disk. Lower values of α will limit the outward transport of equilibrated water from the inner hot region. In this situation, the $(D/H)_{water}$ in the outermost region will be higher than that in

the innermost region, but still be lower than that in the regions where pristine deuterated water is directly accreted. This means that the non-monotonic distribution of $(D/H)_{water}$ will still develop. After infall stops, the less efficient mixing between $(D/H)_{water}$ in different regions will allow the non-monotonic distribution to be preserved for a longer time period, though dust growth could alter this in the long run (Jacquet and Robert, 2013). Conversely, larger values of α would allow the non-monotonic distribution of $(D/H)_{water}$ to continue to exist during the infall stage, but be easily smoothed out after infall stops due to higher level of dynamical mixing.

The primary input parameter related purely to the deuterium chemistry in our model is the initial $(D/H)_{water}$ value in the molecular cloud. Its value would affect the $(D/H)_{water}$ in those regions where the temperature is not high enough for deuterated water to get rapidly isotopically equilibrated with other hydrogen-bearing species. However, while different assumed initial $(D/H)_{water}$ values may lead to differences in absolute values, they will not change the shape of the $(D/H)_{water}$ profile. Thus the non-monotonic distribution of $(D/H)_{water}$ will persist regardless of the initial value in the cloud.

Therefore, the result showing $(D/H)_{water}$ is not monotonic in its distribution with distance from the Sun is expected to be robust. Some differences in the details of the distribution are expected as the region of elevated D/H ratios and the duration over which gradients exist in the disk will vary with the parameters in the model. Future high resolution mapping of protoplanetary disks by ALMA or the measurement of $(D/H)_{water}$ in a wide array comets may allow us begin to constrain what these parameters were in our own or other protoplanetary systems.

4. Discussion

Here we focus on how the distribution of $(D/H)_{water}$ in a protoplanetary disk evolves with time, as D–H exchange occurs between water and other hydrogen-bearing species, while those species are redistributed during the formation and viscous evolution of the disk. As shown above, the $(D/H)_{water}$ reaches relatively low values that approach the bulk (D/H) in the hot inner disk because isotopic exchange is rapid under these conditions and the isotopic fractionations between species are small. The ratio then increases toward the outer disk as the water incorporated at these distances experiences lower temperatures, and therefore undergoes less isotopic exchange with other hydrogen-bearing species. This is consistent with previous studies (e.g., Drouart et al., 1999; Mousis et al., 2000). However, here we find that this increase in the $(D/H)_{water}$ is likely not monotonic, particularly early in disk evolution. Instead, the $(D/H)_{water}$ decreases again in the outermost region, as water that was incorporated early into the disk near the young star would have been pushed outward during the early evolution of the disk. Thus, water ice in the outer regions of the disk may record relatively low (D/H) ratios despite the very low temperatures there. After infall stops, this non-monotonic distribution of solar $(D/H)_{water}$ is slowly erased due to dynamical mixing and transport within the disk.

Accordingly, our study suggests that water ice that was incorporated into cometary bodies early in Solar System evolution could have preserved this non-monotonic distribution of $(D/H)_{water}$. This evolution could explain the recent observations showing that the $(D/H)_{water}$ of a JFC, 103P/Hartley 2, is less than that of previously measured Oort cloud comets (Hartogh et al., 2011), given that JFCs may have formed in the outermost solar nebula (Dones et al., 2004; Morbidelli, 2005; Duncan, 2008). While the formation region of Oort cloud comets is uncertain (Dones et al., 2004; Gomes et al., 2008; Levison et al., 2010; Brasser et al., 2012), the similar $(D/H)_{water}$ of Oort cloud comets and the water found on Saturn's moon Enceladus (Waite et al., 2009) does offer support for the idea that these comets formed from the same reservoir of material as the giant planets, and one that was distinct from the JFCs formation reservoir. Further observations of JFCs and Oort cloud comets will provide better constraints on the extent of $(D/H)_{water}$ variations among these different populations.

An important issue to consider in the future is whether water ice in the outer disk can be further deuterated as a result of the photochemistry, ion-neutral reactions and gas–grain reactions that are expected to become important at the later stages of disk evolution (Aikawa and Herbst, 2001; Willacy, 2007; Willacy and Woods, 2009). Certainly, subsequent photo- and cosmic ray induced chemistry could have occurred in the solar disk, though the effects would have been most important when surface densities were low and mixing had probably homogenized much of the outer disk. Accounting for these effects in future models will result in a more complete understanding of the evolution of $(D/H)_{water}$ in protoplanetary disks.

While this work has focused on the D/H ratio of water, should the scenario we described here have played a role in shaping our Solar System, we should expect to see similar variations in other cometary components. Dullemond et al. (2006) used a similar model to show that the crystallinity of silicate grains would be high in the very outer regions of a protoplanetary disk since the crystalline grains formed in the hot, inner region of the disk at early times could also be subject to efficient outward transport along with the rapid radial expansion of the disk. Later added amorphous interstellar materials would dilute the crystalline fraction at intermediate radial distances. Observations have shown a diversity in the crystalline silicate fraction among Oort cloud comets (Wooden et al., 1999; Kelley et al., 2007), which could be explained in the context of the Dullemond et al. (2006) results. We would thus expect there to be a correlation in comets, with those containing high fractions of crystalline dust also having low $(D/H)_{water}$, as the silicates and ice would both have largely come from the high temperature region of the solar nebula. Further studies aiming to understand the detailed correlations expected between $(D/H)_{water}$ with crystalline/amorphous silicates ratio of comets will allow us to further test and constrain our model.

In conclusion, this work has provided new insights into possible causes of D/H variations in water in the Solar System. Particularly as previous models typically assume a constant $(D/H)_{water}$ as a starting point throughout the disk, we, on the other hand, have shown here that such an assumption is probably not valid as the processing and dynamics of infalling molecular cloud material is likely to create chemical and isotopic gradients in the early solar nebula.

Acknowledgments

We are grateful for valuable, in-depth reviews by F. Hersant, F. Robert and the editor A. Morbidelli, whose suggestions and comments greatly improved the manuscript.

Appendix A

In the chemical network, there are some subsets of coupled reactions, like

$$HD + OH \overset{k_6^+, k_6^-}{\leftrightarrow} H_2O + D$$

$$H_2O + H \overset{k_1^+, k_1^-}{\leftrightarrow} OH + H_2$$

$$H_2 + D \overset{k_4^+, k_4^-}{\leftrightarrow} HD + H$$

Table A1
Reactions and their rate coefficients used in our chemistry network.

No.	Reaction	Rate coefficient ($cm^3\ s^{-1}$)
1, 2	$H_2O + H \leftrightarrow OH + H_2$	$k_1^+ = 1.59\times10^{-11}\times(T/300)^{1.2}\times\exp(-9610/T)$ [1]
		$k_1^- = 2.05\times10^{-12}\times(T/300)^{1.52}\times\exp(-1736/T)$ [1]
3, 4	$H_2 + O \leftrightarrow OH + H$	$k_2^+ = 3.14\times10^{-13}\times(T/300)^{2.7}\times\exp(-3150/T)$ [1]
		$k_2^- = 7\times10^{-14}\times(T/300)^{2.8}\times\exp(-1950/T)$ [1]
5, 6	$H_2O + O \leftrightarrow OH + OH$	$k_3^+ = 1.85\times10^{-11}\times(T/300)^{0.95}\times\exp(-8571/T)$ [1]
		$k_3^- = 1.65\times10^{-12}\times(T/300)^{1.14}\times\exp(-50/T)$ [1]
7, 8	$H_2 + D \leftrightarrow HD + H$	$k_4^+ = 7.5\times10^{-11}\exp(-3820/T)$ [2]
		$k_4^- = 7.5\times10^{-11}\times\exp(-4240/T)$ [2]
9, 10	$HDO + O \leftrightarrow OD + OH$	$k_5^+ = k_3^+$ [3]
		$k_5^- = K_3^-$ [3]
11, 12	$HD + OH \leftrightarrow H_2O + D$	$k_6^+ = 2.12\times10^{-13}\times(T/300)^{2.7}\times\exp(-1258/T)$ [4]
		$k_6^- = k_6^+/k_6$
		where $K_6 = 1/(K_1\cdot K_4)\approx 1/((k_1^+/k_1^-)\cdot(k_4^+/k_4^-))$ [5]
13, 14	$H_2 + OD \leftrightarrow HDO + H$	$k_7^+ = 1.55\times10^{-12}\times(T/300)^{1.6}\times\exp(-1663/T)$ [4]
		$k_7^- = k_7^+/K_7$
		where $K_7 = K_2/K_5\approx(k_2^+/k_2^-)/(k_5^+/k_5^-)$ [5]
15, 16	$OH + D \leftrightarrow H + OD$	$k_8^+ = 9.07\times10^{-11}\times(T/300)^{0.63}$ [6]
		$k_8^- = 1.26\times10^{-10}\times(T/300)^{0.63}\times\exp(-717/T)$ [6]
17, 18	$HD + OH \leftrightarrow HDO + H$	$k_9^+ = 0.6\times10^{-13}\times(T/300)^{1.9}\times\exp(-1258/T)$ [4]
		$k_9^- = k_9^+/K_9$ where $K_9 = K_7\cdot K_8/K_4$ [5]
19, 20	$O + HD \leftrightarrow H + OD$	$k_{10}^+ = 1.57\times10^{-12}\times(T/300)^{1.7}\times\exp(-4639/T)$ [7]
		$k_{10}^- = k_{10}^+/K_{10}$ where $K_{10} = K_2\cdot K_8/K_4$ [5]
20, 21	$O + HD \leftrightarrow D + OH$	$k_{11}^+ = 9.01\times10^{-13}\times(T/300)^{1.9}\times\exp(-3730/T)$ [7]
		$k_{11}^- = k_{11}^+/K_{11}$ where $K_{11} = K_2/K_4$ [5]
22, 23	$O_2 + H \leftrightarrow O + OH$	$k_{12}^+ = 2.61\times10^{-10}\times\exp(-8156/T)$ [1]
		$k_{12}^- = 1.77\times10^{-11}\times\exp(-178/T)$ [1]
24	$O_2 + H_2 \rightarrow OH + OH$	$k_{13} = 3.16\times10^{-10}\times\exp(-21,890/T)$ [1]
25, 26	$O_2 + D \leftrightarrow OD + O$	$k_{14}^+ = 2.61\times10^{-10}\times\exp(-8156/T)$ [3]
		$k_{14}^- = k_{14}^+/K_{14}$ where $K_{14} = K_{12}\cdot K_8$ [5]
27, 28	$H_2 + H_2 \leftrightarrow H_2 + H + H$	$k_{15}^+ = 5.48\times10^{-9}\times\exp(-53,000/T)$ [8]
		$k_{15}^- = 5.5\times10^{-29}\times T^{-1}/8$[a] [9]
29, 30	$H_2 + H \leftrightarrow H + H + H$	$k_{16}^+ = 3.52\times10^{-9}\times\exp(-43,900/T)$ [8]
		$k_{16}^- = 5.5\times10^{-29}\times T^{-1}$[a] [9]
31	$H_2 + He \rightarrow He + H + H$	$k_{17} = 10^{-2.729-23.474/T}\times T^{-1.75}$ [10]
32, 33	$H_2 + HD \leftrightarrow H_2 + D + H$	$k_{18}^+ = k_{15}^+$ [3]
		$k_{18}^- = k_{15}^-$ [3]
34, 35	$H + HD \leftrightarrow H + D + H$	$k_{19}^+ = k_{16}^+$ [3]
		$k_{19}^- = k_{16}^-$ [3]
36	$He + HD \rightarrow He + H + D$	$k_{20} = k_{17}$ [3]
37, 38	$OH + CO \leftrightarrow CO_2 + H$	$k_{21}^+ = 2.81\times10^{-13}\times\exp(-176/T)$ [1]
		$k_{21}^- = 3.38\times10^{-10}\times\exp(-13,163/T)$ [1]
39, 40	$OD + CO \leftrightarrow CO_2 + D$	$k_{22}^+ = k_{21}^+$ [3]
		$k_{22}^- = k_{22}$ where $K_{22} = K_{21}/K_8$ [5]
41, 42	$OH + C \leftrightarrow CO + H$	$k_{23}^+ = 1\times10^{-10}$ [1]
		$k_{23}^- = 1\times10^{-10}\times(T/300)^{0.5}\times\exp(-77,700/T)$ [1]
43, 44	$CO + D \leftrightarrow OD + C$	$k_{24}^+ = k_{23}^-$ [3]
		$k_{24}^- = k_{24}^+/K_{24}$ where $K_{24} = K_8/K_{23}$ [5]
45, 46	$CO + O_2 \leftrightarrow CO_2 + O$	$k_{25}^+ = 5.99\times10^{-12}\times\exp(-24,075/T)$ [1]
		$k_{25}^- = 2.46\times10^{-11}\times\exp(-26,567/T)$ [1]
47, 48	$O_2 + C \leftrightarrow CO + O$	$k_{26}^+ = 2.48\times10^{-12}\times(T/300)^{1.54}\times\exp(613/T)$ [1]
		$k_{26}^- = 2.90\times10^{-11}\times(T/300)^{0.5}\times\exp(-69,300/T)$ [1]

[1] UMIST, Woodall et al. (2007) (by measurements or calculation); [2] Zhang and Miller (1989) (by calculation); [3] assumed; [4] Talukdar et al. (1996) (by measurements); [5] modified for this study—see text; [6] Yung et al. (1988) (by calculation); [7] Joseph et al. (1988) (by calculation); [8] Lepp and Shull (1983) (by calculation); [9] Palla et al. (1983) (by measurements); [10] Dove et al. (1987) (by calculation).

[a] Reaction is third order, so the rate coefficient unit is: $cm^6\ s^{-1}$.

Assuming that the three reversible reactions would reach equilibrium, the equilibrium constant for the first reaction, K_6, would be related to those of the other two, K_1 and K_4 as

$$K_6 = \frac{[H_2O][D]}{[HD][OH]} = \frac{[H_2O][H]}{[H_2][OH]}\cdot\frac{[H_2][D]}{[HD][H]} = 1\Big/\left(\frac{[H_2][OH]}{[H_2O][H]}\cdot\frac{[HD][H]}{[H_2][D]}\right) = 1/(K_1\cdot K_4) \quad \text{(A1)}$$

The equilibrium constant could be estimated as the ratio of corresponding forward and reverse rate constants, $K_6\approx k_6^+/k_6^-$, $K_1\approx k_1^+/k_1^-$, and $K_4\approx k_4^+/k_4^-$. We take k_1^+, k_1^- from the UMIST database while k_4^+, k_4^- were determined by Zhang and Miller (1989), and k_6^+ was studied by Talukdar et al. (1996). If k_6^- is assumed to equal k_1^+ [as was done by Thi et al. (2010)], the relation (A1) would be violated. Thus we modified k_6^- by setting $k_6^- = k_6^+/K_6$ (where $K_6 = 1/(K_1\cdot K_4)$). More examples are provided

in Table A1). Generally this modification resulted in minor shifts of those rate constants compared to their measured values and certainly would fall within the uncertainties of measurements.

After all necessary modifications, we calculated the equilibrated deuterium fractionation factor, f, between water and hydrogen gases, which is shown in Fig. A1 along with the same expression for the reactions used in Thi et al. (2010) and Richet et al. (1977). Here f is defined as

$$f = \frac{[\mathrm{HDO}]/[\mathrm{H_2O}]}{[\mathrm{HD}]/[\mathrm{H_2}]}$$

which represents the deuteration level of water relative to hydrogen gas when the whole system reaches equilibrium. The f in our model decreases with increasing T, which is qualitatively consistent with Richet et al. (1977) (dashed-line) and Thi et al. (2010) (dash-dotted line). The difference between our study and Thi et al. (2010) is due to the revision of some rate coefficients as described above, while the difference between ours and Richet et al. (1977) is caused by different approaches. Richet et al. (1977) predicted the equilibrium values based on thermodynamic calculation and this served as the equilibrium constant for the net D–H exchange reaction in previous studies (Lécluse and Robert, 1994; Drouart et al., 1999; Mousis et al., 2000). Most of the rate constants used in our study are from the UMIST astrochemistry database (Woodall et al., 2007). Given that these reaction rate constants have uncertainties, we calculated the equilibrium f value by changing all reaction rate constants to the maximum and minimum values within the reported uncertainties. These calculations are also shown in Fig. A1, where the dark solid line represents our fiducial model, while the gray region represents the region that is bounded by the uncertainties of the reaction rates. Note that the Richet et al. (1977) value largely falls within this bracketed region, suggesting agreement within the uncertainties.

In detail, the bulk isotopic exchange of hydrogen isotopes between water and molecular hydrogen through our chemical network proceeds faster than that via the reaction $H_2O + HD \leftrightarrow HDO + H_2$ (Lécluse and Robert, 1994). The causes of the disagreement between the Lécluse and Robert (1994) rates and the net exchange rates produced by the reactions in the UMIST database should be considered in future studies. This inconsistency might be caused by uncertainties in the extrapolation of the reaction rates from experiments performed under different temperatures or pressures. Further, some reaction rate coefficients provided by the UMIST database are calculated or extrapolated from reactions involving other isotopologues. While the different chemical schemes yield different results in detail, they both yield similar results in our models. That is, as shown in Fig. A2, the same qualitative behavior is seen in spatial and temporal variations of $(D/H)_{water}$ if we adopt the reaction and rates from Lécluse and Robert (1994) and ignore any other possible reactions involving H, C, or O-bearing species.

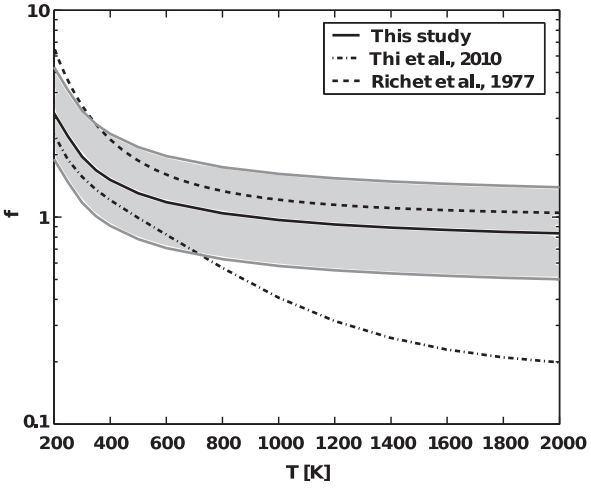

Fig. A1. This figure shows how the isotopic fractionation factor f increases with decreasing T. The solid line indicates this study. The shaded region shows the upper and lower limits of f as a function of temperature, which is caused by the uncertainties in the reaction rate constants adopted in our study. The dashed line represents the equilibrium constant between water and molecular hydrogen calculated by Richet et al. (1977). The dash-dotted line is from Thi et al. (2010) (with only neutral–neutral reactions).

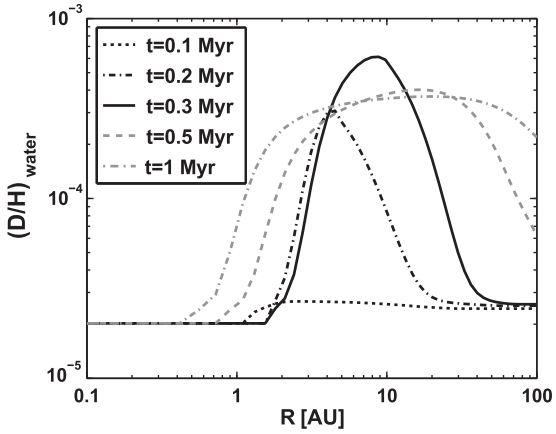

Fig. A2. This figure shows the distribution of D/H of water in the disk at different times. This case uses the isotopic exchange rate used by Drouart et al. (1999), Mousis et al. (2000). As shown, the non-monotonic distribution we find in our model would be still seen.

Appendix B

In the model described in main text (here denoted as model A), the deuterium chemistry is only evaluated at the disk midplane. Since the chemical reaction rates depend sensitively on temperature and pressure, evaluating the chemistry only at the disk midplane would possibly overestimate the rates of isotopic exchange, given that the gas densities decrease by orders of magnitude from the disk midplane to the disk surface and temperature also varies in the vertical direction. Thus, we also applied our dynamical model to explore how radial variations in isotopic ratios would evolve if we accounted for the vertical structure of the disk in a viscously evolving disk (denoted as model B).

B.1. Disk vertical structure

We use the same dynamical model described in model A to calculate how the disk evolves over time. Knowing $\Sigma(R, t)$ at a given time, the vertical structure of the gas is found by assuming that the disk stays in hydrostatic equilibrium:

$$\frac{\partial P(R,z,t)}{\partial z} = -g_z \rho(R,z,t) = -\Omega^2 z \rho(R,z,t) \qquad \text{(A2)}$$

where g_z is the vertical component of gravity acceleration, Ω is the Keplerian angular velocity at location R in the disk, and pressure, $P(R,z,t) = \rho(R,z,t)C_s^2$ (where $C_s = (R_g T/\mu)^{1/2}$, R_g is the molar gas constant and μ is the mean molecular weight) according to the ideal gas equation of state. Here, for simplification, C_s is assumed to be

constant in the vertical direction. As a result, the volume density would vary in the vertical direction following the description as

$$\rho(R,z,t) = \rho_c(R,z,t)\exp\left(-\frac{z^2}{2H^2}\right) \quad \text{(A3)}$$

where $\rho_c(R,t) = \Sigma(R,t)/(\sqrt{2\pi}H)$ is the volume density at disk midplane, and H is the vertical scale height ($H = C_s/\Omega$). This treatment has a caveat which will be discussed further below.

As for the vertical thermal structure, the temperature gradient is described as

$$\frac{\partial T(R,z,t)}{\partial z} = -\frac{3\kappa\rho(R,z,t)F_{rad}}{16\sigma T(R,z,t)^3} \quad \text{(A4)}$$

where κ is the disk opacity, F_{rad} is radiation flux along the vertical direction, and σ is the Stefan–Boltzmann constant. In model B, F_{rad} is assumed to be constant in the vertical direction and equals the flux of radiation from disk surface.

Thus, temperatures are highest at the disk midplane, where viscous dissipation rates are largest, and they decrease with height. As a result of these temperature and pressure variations, we expect isotopic exchange to be most rapid at the disk midplane, and to become more sluggish with increasing height. This may not be true in the case where the stellar irradiation is important, leading to much higher temperatures at the disk surface than at the midplane. However, this is generally true in the low density, low temperature regions of the disk where the chemistry is very sluggish. Thus, focusing purely on a viscous disk suffices to capture the effects of chemical variations.

We also performed calculations where we allowed the radiation flux to vary with height (Pringle, 1981):

$$\frac{\partial F(R,z,t)}{\partial z} = \frac{9}{4}\nu\Omega^2\rho \quad \text{(A5)}$$

and calculated the vertical structure in a completely self-consistent manner as in Dodson-Robinson et al. (2009) and Vasyunin et al. (2011). Again, because most of the processing took place around the disk midplane, minimal differences in the D–H exchange were noted. As a result, using the simplified model still allows for a reasonable approximation to the conditions in which isotopic exchange would occur in the early solar nebula, and is computationally less demanding, and as such, was the primary approach used here. Any differences in results that arise to differences in the vertical structure of the disk appear small compared to all other uncertainties that arise from choices of the main parameters in the model.

B.2. Numerical approach of model B

A step-wise summary of model B is provided in Fig. A3. The disk surface density $\Sigma(R,t)$ and midplane temperature $T_m(R,t)$ are computed with the same method as that used in model A. During each timestep, the vertical variations in density and temperature, $\rho(R,z,t)$ and $T(R,z,t)$ are computed from the midplane up to 6H at 6 equally spaced levels. The change in chemistry is evaluated at each level, with the number density of each species in Eq. (3) related to its density by $[i] = \rho_i(R,z,t)/m_i$. Then the new surface density of each species at location R is calculated by integrating the new abundances over the height of the disk using Simpson's algorithm, and is taken as the initial value of the next timestep. While we adopt a coarse vertical resolution here for the sake of reducing computational time, this resolution suffices to provide insights into how allowing for the vertical variation in gas properties affects the isotopic evolution of materials.

B.3. Model results

We applied this methodology to the same cloud collapse and disk model described in the manuscript, with the same values of ω_{cd}, T_{cd}, α as adopted in the standard model (referring to Tables 1–3). Thus, the disk physical evolution is the same as what was shown in Fig. 3 in the main text.

As shown in Fig. A4, water in the inner hot region still rapidly equilibrates with the other species, with minimal differences in

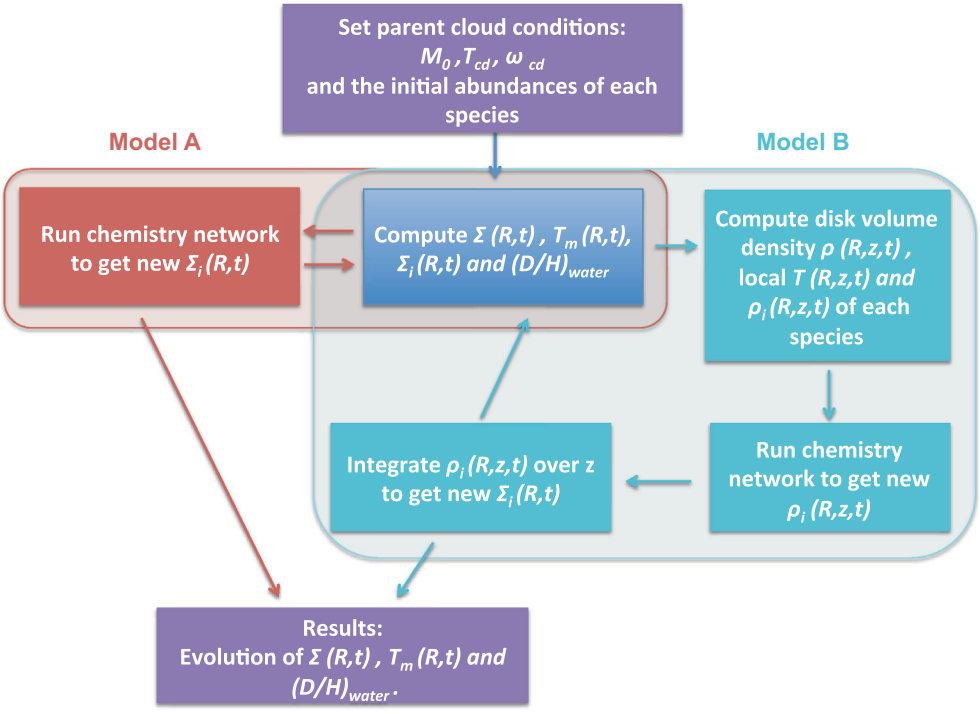

Fig. A3. This figure shows the comparison of algorithms used in the model described in main text (model A) and the 1 + 1D model described in Appendix B (model B).

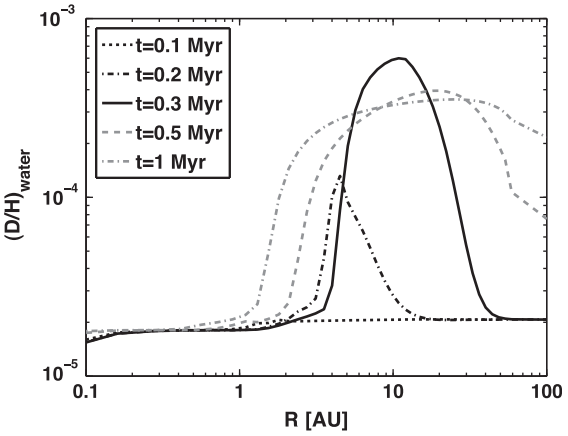

Fig. A4. The distribution of $(D/H)_{water}$ in the solar nebula at different times as predicted from our 1 + 1D model. Again, the black lines represent the time during the infall stage, and the gray lines show the $(D/H)_{water}$ profiles once infall has ceased.

the isotopic ratios reached further out in the disk. Again, as the equilibrated water with low (D/H) values from the inner hot region would have been transported to the outermost region by the viscous spreading, a similar distribution of $(D/H)_{water}$ in the solar nebula during the earlier stages of disk evolution as predicted in the main text is also seen in the 1 + 1D model. As such, we do not expect a detailed vertical structure model to affect our conclusions.

References

Aikawa, Y., Herbst, E., 2001. Two-dimensional distributions and column densities of gaseous molecules in protoplanetary disks. II. Deuterated species and UV shielding by ambient clouds. Astron. Astrophys. 371, 1107–1117.

Armitage, P.J., Livio, M., Pringle, J.E., 2001. Episodic accretion in magnetically layered protoplanetary discs. Mon. Not. R. Astron. Soc. 324, 705–711.

Balsiger, H., Altwegg, K., Geiss, J., 1995. D/H and O-18/O-16 ratio in the hydronium ion and in neutral water from in situ ion measurements in comet Halley. J. Geophys. Res. 100, 5827–5834.

Bergin, E.A., Phillips, T.G., Comito, C., et al., 2010. Herschel observations of EXtra-Ordinary Sources (HEXOS): The present and future of spectral surveys with Herschel/HIFI. Astron. Astrophys. 521, L20.

Bockelée-Morvan, D., Gautier, D., Lis, D.C., Young, K., Keene, J., Phillips, T., Owen, T., Crovisier, J., Goldsmith, P.F., Bergin, E.A., Despois, D., Wootten, A., 1998. Deuterated water in Comet C/1996 B2 (Hyakutake) and its implications for the origin of comets. Icarus 133, 147–162.

Bockelée-Morvan, D. et al., 2012. Herschel measurements of the D/H and $^{16}O/^{18}O$ ratios in water in the Oort-cloud Comet C/2009 P1 (Garradd). Astron. Astrophys. 544, L15.

Brasser, R., Duncan, M.J., Levison, H.F., Schwamb, M.E., Brown, M.E., 2012. Reassessing the formation of the inner Oort cloud in an embedded star cluster. Icarus 217, 1–19.

Brown, P.D., Millar, T.J., 1989. Models of the gas–grain interaction – Deuterium chemistry. Mon. Not. R. Astron. Soc. 237, 661–671.

Brown, R.H., Lauretta, D.S., Schmidt, B., Moores, J., 2012. Experimental and theoretical simulations of ice sublimation with implications for the chemical, isotopic, and physical evolution of icy objects. Planet. Space Sci. 60, 166–180.

Cassen, P., 1994. Utilitarian models of the solar nebula. Icarus 112, 405–429.

Cassen, P., 2001. Nebular thermal evolution and the properties of primitive planetary materials. Meteorit. Planet. Sci. 36, 671–700.

Ciesla, F.J., Cuzzi, J.N., 2006. The evolution of the water distribution in a viscous protoplanetary disk. Icarus 181, 178–204.

Coutens, A. et al., 2012. A study of deuterated water in the low-mass protostar IRAS 16293-2422. Astron. Astrophys. 539, 132–143.

Cuzzi, J.N., Zahnle, K.J., 2004. Material enhancement in protoplanetary nebulae by particle drift through evaporation fronts. Astrophys. J. 614, 490–496.

Cyr, K.E., Sears, W.D., Lunine, J.I., 1998. Distribution and evolution of water ice in the solar nebula: Implications for Solar System body formation. Icarus 135, 537–548.

De Laeter, J.R. et al., 2003. Atomic weights of the elements: Review 2000 (IUPAC technical report). Pure Appl. Chem. 75, 683–800.

Dodson-Robinson, S., Willacy, K., Bodenheimer, P., Turner, N.J., Beichman, C.A., 2009. Ice lines, planetesimal composition and solid surface density in the solar nebula. Icarus 200, 672–693.

Dones, L., Weissman, P.R., Levison, H.F., Duncan, M.J., 2004. Oort cloud formation and dynamics. In: Festou, M. et al. (Eds.), Comets II. University of Arizona Press, Tucson, pp. 153–174.

Dove, J.E., Rusk, A.C.M., Cribb, P.H., Martin, P.G., 1987. Excitation and dissociation of molecular hydrogen in shock waves at interstellar densities. Astrophys. J. 318, 379–391.

Drouart, A., Dubrulle, B., Gautier, D., Robert, F., 1999. Structure and transport in the solar nebula from constraints on deuterium enrichment and giant planets formation. Icarus 140, 129–155.

Dullemond, C.P., Apai, D., Walch, S., 2006. Crystalline silicates as a probe of disk formation history. Astrophys. J. Lett. 640, L67–L70.

Duncan, M.J., 2008. Dynamical origin of comets and their reservoirs. Origin and Early Evolution of Comet Nuclei, Space Sciences Series of ISSI, vol. 28. Springer Science + Business Media, pp. 109–126.

Gammie, C.F., 1996. Layered accretion in T Tauri disks. Astrophys. J. 457, 355–362.

Geiss, J., Gloeckler, G., 1998. Abundances of deuterium and helium-3 in the protosolar cloud. Space Sci. Rev. 84, 239–250.

Geiss, J., Reeves, H., 1981. Deuterium in the Solar System. Astron. Astrophys. 93, 189–199.

Gensheimer, P.D., Mauersberger, R., Wilson, T.L., 1996. Water in galactic hot cores. Astron. Astrophys. 314, 281–294.

Gomes, R.S., Fern Ndez, J.A., Gallardo, T., Brunini, A., 2008. The scattered disk: Origins, dynamics, and end states. In: Barucci, M.A., Boehnhardt, H., Cruikshank, D.P., Morbidelli, A. (Eds.), The Solar System beyond Neptune. University of Arizona Press, Tucson, pp. 259–273.

Goodman, A.A., Benson, P.J., Fuller, G.A., Myers, P.C., 1993. Dense cores in dark clouds. VIII – Velocity gradients. Astrophys. J. 406, 528–547.

Hartmann, L., Calvet, N., Gullbring, E., D'Alessio, P., 1998. Accretion and the evolution of T Tauri disks. Astrophys. J. 495, 385–410.

Hartogh, P. et al., 2011. Ocean-like water in the Jupiter-family Comet 103P/Hartley 2. Nature 478, 218–220.

Hersant, F., Gautier, D., Huré, J., 2001. A two-dimensional model for the primordial nebula constrained by D/H measurements in the Solar System: Implications for the formation of giant planets. Astrophys. J. 554, 391–407.

Horner, J., Mousis, O., Hersant, F., 2007. Constraints on the formation regions of comets from their D:H ratios. Earth Moon Planets 100, 43–56.

Hueso, R., Guillot, T., 2005. Evolution of protoplanetary disks: Constraints from DM Tauri and GM Aurigae. Astron. Astrophys. 442, 703–725.

Jacq, T., Walmsley, C.M., Henkel, C., Baudry, A., Mauersberger, R., Jewell, P.R., 1990. Deuterated water and ammonia in hot cores. Astron. Astrophys. 228, 447–470.

Jacquet, E., Robert, F., 2013. Water transport in protoplanetary disks and the hydrogen isotopic composition of chondrites. Icarus 223, 722–732.

Joseph, T., Truhlar, D.G., Garrett, B.C., 1988. Improved potential energy surfaces for the reaction $O(3P) + H_2 \rightarrow OH + H$. J. Chem. Phys. 88 (11), 6982–6990.

Kavelaars, J.J., Mousis, O., Petit, J., Weaver, H.A., 2011. On the formation location of Uranus and Neptune as constrained by dynamical and chemical models of comets. Astrophys. J. Lett. 734, L30–L34.

Kelley M.S., Harker D.E., Wooden D.H., Woodward C.E., 2007. Crystalline silicates and the specular comet C/2006 P1 (McNaught). AAS Meeting. Bull. Am. Astron. Soc., 39, pp. 827.

Lécluse, C., Robert, F., 1994. Hydrogen isotope exchange reaction rates: Origin of water in the inner Solar System. Geochim. Cosmochim. Acta 58, 2927–2939.

Lepp, S., Shull, J.M., 1983. The kinetic theory of H_2 dissociation. Astrophys. J. 270, 578–582.

Lerate, M.R. et al., 2006. A far-infrared molecular and atomic line survey of the Orion KL region. Mon. Not. R. Astron. Soc. 370, 597–628.

Levison, H.F., Duncan, M.J., Brasser, R., Kaufmann, D.E., 2010. Capture of the Sun's Oort cloud from stars in its birth cluster. Science 329, 187–190.

Linsky, J.L., 2003. Atomic deuterium/hydrogen in the Galaxy. Space Sci. Rev. 106, 49–60.

Liu, F.-C., Parise, B., Kristensen, L., Visser, R., van Dishoeck, E.F., Güsten, R., 2011. Water deuterium fractionation in the low-mass protostar NGC1333-IRAS2A. Astron. Astrophys. 527, 19–24.

Lodato, G., 2008. Classical disc physics. New Astron. Rev. 52, 21–41.

Lodders, K., 2010. Solar System abundances of the elements. In: Goswami, A., Reddy, B.E. (Eds.), Principles and Perspectives in Cosmochemistry. Astrophysics and Space Science Proceedings. Springer, New York, pp. 379–417.

Lynden-Bell, D., Pringle, J.E., 1974. The evolution of viscous discs and the origin of the nebular variables. Mon. Not. R. Astron. Soc. 168, 603–637.

Meier, R. et al., 1998. A determination of the HDO/H_2O ratio in Comet C/1995 O1 (Hale-Bopp). Science 279, 842–844.

Millar, T.J., 2002. Modelling deuterium fractionation in interstellar clouds. Planet. Space Sci. 50, 1189–1195.

Millar, T.J., Bennett, A., Herbst, E., 1989. Deuterium fractionation in dense interstellar clouds. Astrophys. J. 340, 906–920.

Morbidelli, A., 2005. Origin and Dynamical Evolution of Comets and their Reservoirs. ArXiv Astrophysics e-prints: 12256.

Mousis, O., Gautier, D., Bockelée-Morvan, D., Robert, F., Dubrulle, B., Drouart, A., 2000. Constraints on the formation of comets from D/H ratios measured in H_2O and HCN. Icarus 148, 513–525.

Palla, F., Salpeter, E.E., Stahler, S.W., 1983. Primordial star formation: The role of molecular hydrogen. Astrophys. J. 271, 632–641.

Persson, C.M. et al., 2007. A spectral line survey of Orion KL in the bands 486–492 and 541–577 GHz with the Odin satellite. II. Data analysis. Astron. Astrophys. 476, 807–827.

Petit, J.-M., Kavelaars, J.J., Mousis, O., Weaver, H.A., 2011. Formation location of Uranus and Neptune from D/H in satellites and comets. In: EPSC-DPS Joint Meeting 2011, held 2–7 October 2011 in Nantes, France, pp. 1442.
Pringle, J.E., 1981. Accretion discs in astrophysics. Annu. Rev. Astron. Astrophys. 19, 137–162.
Richet, P., Bottinga, Y., Janoy, M., 1977. A review of hydrogen, carbon, nitrogen, oxygen, sulphur, and chlorine stable isotope enrichment among gaseous molecules. Annu. Rev. Earth Planet. Sci. 5, 65–110.
Robert, F., 2006. Solar System deuterium/hydrogen ratio. In: Meteorites and the Early Solar System II, pp. 341–351.
Roberts, H., Millar, T.J., 2000. Modelling of deuterium chemistry and its application to molecular clouds. Astron. Astrophys. 361, 388–398.
Roberts, H., Herbst, E., Millar, T.J., 2004. The chemistry of multiply deuterated species in cold, dense interstellar cores. Astron. Astrophys. 424, 905–917.
Rodgers, S.D., Millar, T.J., 1996. The chemistry of deuterium in hot molecular cores. Mon. Not. R. Astron. Soc. 280, 1046–1054.
Shakura, N.I., Sunyaev, R.A., 1973. Black holes in binary systems. Observational appearance. Astron. Astrophys. 24, 337–355.
Shu, F.H., 1977. Self-similar collapse of isothermal spheres and star formation. Astrophys. J. 214, 488–497.
Talukdar, R.K., Gierczak, T., Goldfarb, L., Rudich, Y., Kao, B.S.M., Ravishankara, A.R., 1996. Kinetics of hydroxyl radical reactions with isotopically labeled hydrogen. J. Phys. Chem. 100, 3037–3043.
Thi, W.-F., Woitke, P., Kamp, I., 2010. Warm non-equilibrium gas phase chemistry as a possible origin of high HDO/H_2O ratios in hot and dense gases: Application to inner protoplanetary discs. Mon. Not. R. Astron. Soc. 407, 232–246.
van Dishoeck, E.F., Blake, G.A., Draine, B.T., Lunine, J.I., 1993. The Chemical Evolution of Protostellar and Protoplanetary Matter, pp. 163–241.
Vasyunin, A.I., Wiebe, D.S., Birnstiel, T., Zhukovska, S., Henning, T., Dullemond, C.P., 2011. Impact of grain evolution on the chemical structure of protoplanetary disks. Astrophys. J. 727, 76–93.
Villanueva, G.L., Mumma, M.J., Bonev, B.P., Di Santi, M.A., Gibb, E.L., Böhnhardt, H., Lippi, M., 2009. A sensitive search for deuterated water in Comet 8p/Tuttle. Astrophys. J. Lett. 690, L5–L9.
Waite, J.H.J. et al., 2009. Liquid water on Enceladus from observations of ammonia and ^{40}Ar in the plume. Nature 460, 487–490.
Weidenschilling, S.J., 1977. Aerodynamics of solid bodies in the solar nebula. Mon. Not. R. Astron. Soc. 180, 57–70.
Willacy, K., 2007. The chemistry of multiply deuterated molecules in protoplanetary disks. I. The outer disk. Astrophys. J. 660, 441–460.
Willacy, K., Woods, P.M., 2009. Deuterium chemistry in protoplanetary disks. II. The inner 30 AU. Astrophys. J. 703, 479–499.
Woodall, J., Agúndez, M., Markwick-Kemper, A.J., Millar, T.J., 2007. The UMIST database for astrochemistry 2006. Astron. Astrophys. 466, 1197–1204.
Wooden, D.H., Harker, D.E., Woodward, C.E., Butner, H.M., Koike, C., Witteborn, F.C., McMurtry, C.W., 1999. Silicate mineralogy of the dust in the inner coma of Comet C/1995 01 (Hale-Bopp) pre- and postperihelion. Astrophys. J. 517, 1034–1058.
Yang, L., Ciesla, F.J., 2012. The effects of disk building on the distributions of refractory materials in the solar nebula. Meteorit. Planet. Sci. 47, 99–119.
Yung, Y.L., Wen, J., Friedl, R.R., Pinto, J.P., Bayes, K.D., 1988. Kinetic isotopic fractionation and the origin of HDO and CH_3D in the Solar System. Icarus 74, 121–132.
Zhang, J.Z.H., Miller, W.H., 1989. Quantum reactive scattering via the S-matrix version of the Kohn variational principle: Differential and integral cross sections for $D + H_2HD + H$. J. Chem. Phys. 91 (3), 1528–1547.
Zhu, Z., Hartmann, L., Gammie, C., 2010. Long-term evolution of protostellar and protoplanetary disks. II. Layered accretion with infall. Astrophys. J. 713, 1143–1158.